

See discussions, stats, and author profiles for this publication at: <https://www.researchgate.net/publication/299997256>

A Tunable Leapfrog Complex Filter for High Frequency and Wide Bandwidth Using Multi-Output Current Differencing Transconductance Amplifiers

Article in IETE Journal of Research · April 2016

DOI: 10.1080/03772063.2016.1164633

CITATIONS

0

READS

46

4 authors, including:



Chunhua Wang

Hunan University

167 PUBLICATIONS 792 CITATIONS

[SEE PROFILE](#)

Some of the authors of this publication are also working on these related projects:



time-delay chaotic system [View project](#)



RF CMOS receiver [View project](#)



A Tunable Leapfrog Complex Filter for High Frequency and Wide Bandwidth Using Multi-Output Current Differencing Transconductance Amplifiers

Hao Peng, Chunhua Wang, Xiaotong Tian & Jun Liu

To cite this article: Hao Peng, Chunhua Wang, Xiaotong Tian & Jun Liu (2016): A Tunable Leapfrog Complex Filter for High Frequency and Wide Bandwidth Using Multi-Output Current Differencing Transconductance Amplifiers, IETE Journal of Research

To link to this article: <http://dx.doi.org/10.1080/03772063.2016.1164633>



Published online: 07 Apr 2016.



Submit your article to this journal [↗](#)



View related articles [↗](#)



View Crossmark data [↗](#)



A Tunable Leapfrog Complex Filter for High Frequency and Wide Bandwidth Using Multi-Output Current Differencing Transconductance Amplifiers

Hao Peng¹, Chunhua Wang¹, Xiaotong Tian¹ and Jun Liu²

¹College of Computer Science and Electronic Engineering, Hunan University, Changsha, P.R.China; ²STATE GRID HUNAN electric power company, Changsha, P.R.China

ABSTRACT

In this paper, a new fourth-order complex (polyphase) filter is realized with the leapfrog structure. The proposed filter is based on the first-order stage using multi-output current differencing transconductance amplifiers (MOCDTAs). The design procedures for the realization of the first-order stage and fourth-order leapfrog polyphase filter are presented. In the procedures, the signal flow diagrams are also presented. The proposed design using MOCDTA simplifies the circuit of the current-mode leapfrog complex filter, where there are no resistors and with minimum number of active components. Besides, its centre frequency and bandwidth could be electrically tunable independently. The centre frequency of the proposed filter could be adjusted from 20 to 80 MHz, and its bandwidth could be more than 20 MHz. With ± 1.25 V supply, two examples of the proposed filter are introduced. Their bandwidths are from 46.1 to 68.5 MHz and from 22.3 to 48.4 MHz, respectively. Their image rejection ratios could be more than 59 and 39 dB, respectively. Meanwhile, both the IIP3s are over 18 dBm. The theoretical results are demonstrated by using SPECTRE simulation in CHRT 0.18 μm standard complementary metal oxide semiconductor (CMOS) process.

KEYWORDS

Current-mode; Complex filter; Image rejection; Tunable independently, high centre frequency; Leapfrog; MOCDTA

1. INTRODUCTION

The complex (polyphase) filter, known as an important structure for suppressing undesired image signals caused by the down-conversion operation, is widely used in radio frequency (RF) receivers such as intermediate frequency (IF) receivers. Its frequency response is asymmetrical around dc, which results in the image rejection [1]. To obtain this feature, the linear frequency transformation is utilized, and this approach is making the low-pass response into an identical band-pass response. In this approach, the polyphase filter is made up of close cross-coupling of two equal real low-pass filters. The signals which are through the two filters possess equal amplitude and quadrature phase [1].

High-order complex filters have attracted our attention due to their high bandwidth and high image rejection ratio (IRR). In literatures, there are several methods to implement the high-order polyphase filter by employing diverse active components. These methods can be classified into three categories based on their synthesis method. First is to cascade first-order stages without inter-stage feedback in [2–11]. Second is to simulate the high-order LC (circuit is based on inductance [L] and capacitor [C]) prototypes through employing active and passive components in [12–22]. Third is to cascade first-order stages with inter-stage feedback in [1,23].

The first category shows a convenient approach to realize the high-order polyphase filter. However, this approach suffers from some problems. In [7,8,10,11], first-order polyphase filters could obtain just quality factor of one-half for each stage. Thus, additional sections are employed to improve the quality factor. Those sections would be realized usually by using passive or active resistors and they could increase the complexity.

In the second category, the polyphase filter is realized by the simulation of LC prototypes. This approach where more active components are employed makes the filter complicated. In [20], in order to simulate active resistors, differential capacitors and differential inductors, the number of operational transconductance amplifiers (OTAs) is one, two, and four, respectively. Thus, the five-order polyphase filter proposed in [20] employs 32 OTAs.

As [24] describes, the leapfrog (LF) structure is one of the most popular choices in active-RC real filters due to its low sensitivity which is lower than that of the first category, and the number of active components in LF structure could be lower than that in the structure based on LC simulation. Likewise, the LF structure could be adopted to implement high-order complex filter

efficiently, and this is the third category. In [23], the filter employs the LF structure to realize fourth-order filter while using 16 OTAs. It means that additional two OTAs are needed as active resistors to perform feedbacks per each first-order stage.

From above three categories, we can find that the high-order polyphase filter in the third category has some advantages over the one in other categories. In above three categories, many kinds of active component are employed to realize the polyphase filter, such as OTAs in [23], current conveyors in [8], second-generation current conveyors (CCII) in [2,5–7], CCII-based current followers, voltage followers in [3,4,11], and current feedback operation amplifiers in [9,10]. These active components used in the filter could affect the work frequency, that is to say, the IF of the RF receiver which is affected by the work frequency could not be high. Nevertheless, as [3] expounds, in order to avoid increasing the phase-locked loop locking time, folding distortion, and flicker noise the higher IF is significant and necessary in the RF receiver. Besides, these above active components used in the complex filter lead to a common problem that the first-order stage needs redundant active or passive components to improve quality factor. Considering above two points, we should adopt a new component which could not only make filter work at high frequency without increasing the complexity of the filter but also adjust the quality factor without redundant components.

A new current-mode active element, called current differencing transconductance amplifier (CDTA), has been introduced [25]. It has some characteristics such as high output impedance, low input impedance, high linearity, and wide frequency response. Multi-output current differencing transconductance amplifier (MOCDDTA) with multiple outputs is based on CDTA [26]. It contains three transconductance stages which provide independent multiple current outputs. So, the design using MOCDDTA could make that each first-order stage requires only two active component and two capacitors, meanwhile, high quality factor, high output impedance and low input impedance could be achieved. Besides, the MOCDDTA possesses virtual-grounded input ports, which could make MOCDDTA-based polyphase filter work at a high frequency.

In this paper, the concept is based on the employment of MOCDDTA to realize the polyphase filter configurations. For this purpose, the current-mode design approach by which the realization of the first-order stage needs only two active components and two capacitors has been performed, and the synthesis procedure of signal flow

diagram (SFD) of the fourth-order leapfrog complex filter is presented as well. Based on above two points, a fourth-order leapfrog complex filter topology would be introduced. The proposed fourth-order filter is realized with no resistors and with minimum number of active components, and its centre frequency and the bandwidth could be electrically tunable independently. The obtained simulation results confirm their correct operation.

2. CIRCUIT DESIGN AND ANALYSIS

2.1 The Active Component

The circuit symbol of the proposed active component MOCDDTA is shown in Figure 1(a), where P and N are low-impedance current-input terminals, Z , $X+$, $AX\pm$, and $BX\pm$ are high-impedance current-output terminals. This component is equivalent to the circuit in Figure 1(b), which involves dependent current sources at Z , $X+$, $AX\pm$, and $BX\pm$. The MOCDDTA terminal equation can be defined by

$$\begin{bmatrix} V_P \\ V_N \\ V_Z \\ I_Z \\ I_X \\ \pm I_{AX} \\ \pm I_{BX} \end{bmatrix} = \begin{bmatrix} 0 & 0 & 0 & 0 \\ 0 & 0 & 0 & 0 \\ 0 & 0 & Z_Z & 0 \\ 1 & -1 & 0 & 0 \\ 0 & 0 & 0 & \pm g_m \\ 0 & 0 & \pm K_a g_m Z_Z & \pm K_a g_m \\ 0 & 0 & \pm K_b g_m Z_Z & \pm K_b g_m \end{bmatrix} \begin{bmatrix} I_P \\ I_N \\ I_Z \\ V_Z \end{bmatrix} \quad (1)$$

where g_m is the transconductance gain, K_a is the gain coefficient from $X+$ terminal to $AX\pm$ terminals, and K_b is the gain coefficient from $X+$ terminal to $BX\pm$

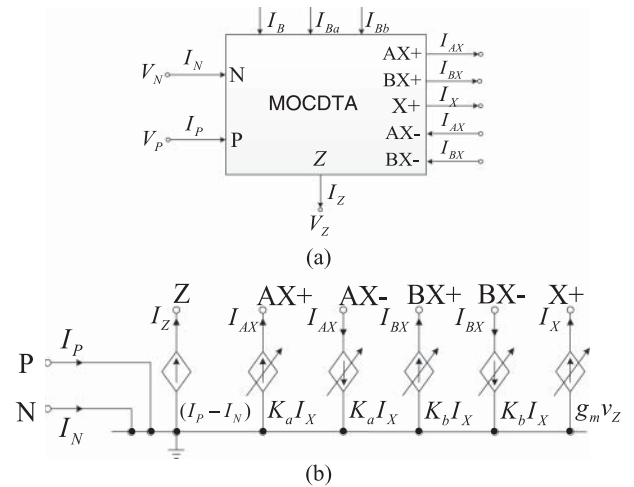


Figure 1: (a) Symbol of MOCDDTA and (b) equivalent circuit of MOCDDTA

terminals. They are directly proportional to the external current I_B , I_{Ba} and I_{Bb} , respectively. According to Equation (1), the current I_Z follows the differencing of the currents through the terminals P and N and flows from the terminal Z into external impedance Z_Z . The voltage drop at terminal Z is transferred to a current at the terminal $X+$ by a transconductance g_m . The current $\pm I_{AX}$ and $\pm I_{BX}$ are transmitted by current gain coefficient K_a and K_b from I_X .

The CMOS-based MOCDDTA circuit is shown in Figure 2, which consists of three transconductance stages and one current differencing stage. In Figure 2, the current differencing stages are realized by the transistors M1–M12, which convey the input currents and realize their subtraction. The transconductance g_m is got by the transconductance stage realized by transistors M13–M26, it could be given as

$$g_m = \sqrt{I_B \mu C_{ox} (W/L)_{M13}} \quad (2)$$

where μ is the mobility of the carriers, C_{ox} is the gate-oxide capacitance per unit area, $(W/L)_{M13}$ is the width to length ratio of the transistor M13. The remaining two transconductance stages are realized by the transistors M27–M40 and M41–M54, respectively. To obtain the current gain coefficient K_a , K_b , two polysilicon resistors

are added at the gates of M27 and M41, respectively. They could be written as

$$K_a = \alpha (L/W)_{\text{PolyR1}} \sqrt{I_{Ba} \mu C_{ox} (W/L)_{M27}} \quad (3)$$

$$K_b = \alpha (L/W)_{\text{PolyR2}} \sqrt{I_{Bb} \mu C_{ox} (W/L)_{M41}} \quad (4)$$

where α is proportional to the ratio of doping density to thickness of the polysilicon, $(W/L)_{M27}$ is the width to length ratio of the transistor M27, $(L/W)_{\text{PolyR1}}$ and $(L/W)_{\text{PolyR2}}$ are the length to width ratio of polysilicon resistor PolyR1 and PolyR2, respectively. According to Equations (2)–(4), the transconductance g_m and current gain K_a , K_b could be adjusted by external bias current I_B , I_{Ba} , and I_{Bb} , respectively. When the $I_{Ba} = I_{Bb} = 40 \mu\text{A}$, the current gain coefficient $K_a = K_b = 1$. We will assume that all MOS devices operate in the saturation region. The dimensions of the metal oxide semiconductor (MOS) transistors used in the MOCDDTA implementation are given in Table 1.

2.2 The First-order Stage

In essence, the first-order stage of a polyphase filter is a complex lossy integrator. The SFD of complex lossy

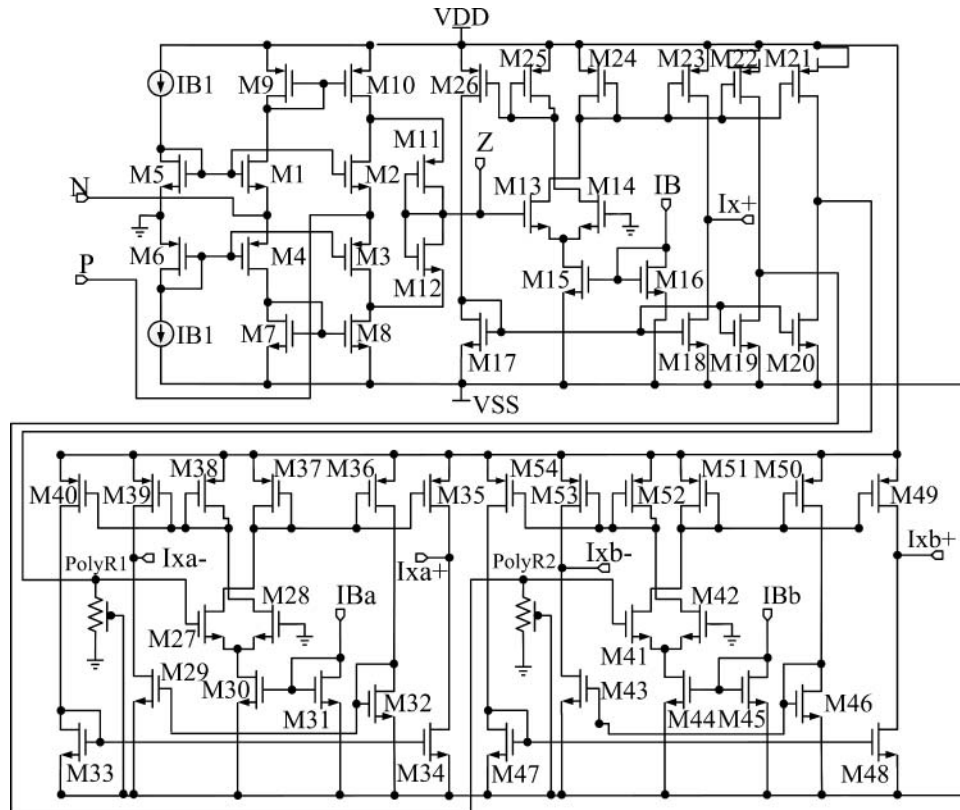


Figure 2: The CMOS realization of MOCDDTA

Table 1: Width to length ratios of the transistors

Transistors	W/L (width to length ratios)
M1–M6	5.6 ($L = 0.36 \mu$)
M7–M10	32 ($L = 1 \mu$)
M11, M12	111 ($L = 0.36 \mu$)
M13, M14, M21–M26, M35–M40, M49–M54	47.6 ($L = 0.42 \mu$)
M17–M20, M29, M32, M33, M34, M43, M46–M48	1.3 ($L = 0.8 \mu$)
M15, M16, M30, M31, M44, M45	5.6 ($L = 0.36 \mu$)
PolyR1, PolyR2	0.16 ($L = 4.95 \mu$)

integrator could be got by the transposition of two real integrators in Figure 3(a). Since the input signals of the two paths have equal amplitude and 90° phase difference, the feedback between the two paths could perform a frequency shift according to $s \rightarrow s - j\omega_c$, where ω_c expresses the frequency shift of the transfer function. So, the transfer function of the first-order stage (complex lossy integrator) is written by

$$H(j\omega) = \frac{I_{oc}}{I_{ic}} = -\frac{\omega_0}{j(\omega - \omega_c) + \omega_0} \quad (5)$$

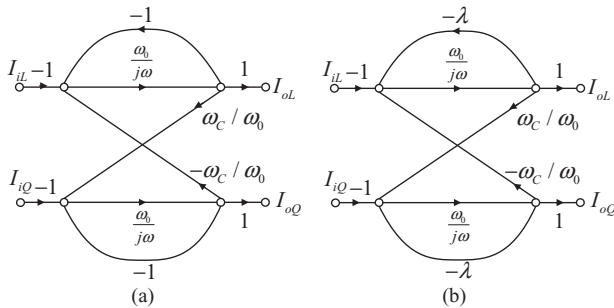
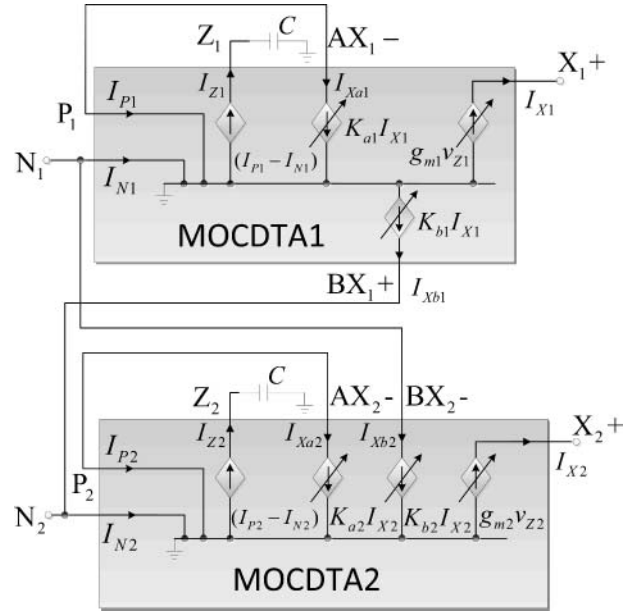
where ω_0 is the cut-off frequency of the real first-order filter. As a frequency shift with $s \rightarrow s - j\omega_c$, the low-pass filter's amplitude-frequency response in negative domain is shifted to positive domain. So, the cut-off frequency is equal to half of the bandwidth of the first-order stage.

In this paper, a modified SFD of a first-order polyphase filter is proposed in Figure 3(b), whose transfer function is written by

$$H_m(j\omega) = \frac{I_{oL}}{I_{iL}} = -\frac{1}{\lambda} \frac{\omega_{m0}}{j(\omega - \omega_c) + \omega_{m0}} \quad (6)$$

where $\omega_{m0} = \lambda\omega_0$. So, the modified polyphase filter's bandwidth ω_{m0} could be adjusted by λ , which provides a possible way to adjust bandwidth and centre frequency independently.

From Figure 1(b), we could observe that there are multiple outputs at MOCDTA. So, the number of the output

**Figure 3: SFD of a first-order filter: (a) detailed transmission and (b) modified transmission****Figure 4: Equivalent circuit for realization of the first-order stage**

is enough to satisfy the feedback of Figure 3(b). Furthermore, the output and input signals of MOCDTA are of current-mode, the signals are convenient to be merged at the node in consequence. The current-mode realization of the SFD of Figure 3(b) is shown in Figure 4 where the topology offers capability for resistorless realization.

In Figure 4, the bias currents and external capacitors of two MOCDTA are equal each other. So, we can assume that $g_{m1} = g_{m2} = g_m$, $K_{a1} = K_{a2} = K_a$, and $K_{b1} = K_{b2} = K_b$. We can get the transfer function of the first-stage in Figure 4, which is rewritten by

$$H_m(j\omega) = -\frac{1}{K_a} \frac{1}{j((C/g_m K_a)\omega - K_b/K_a) + 1} \quad (7)$$

where C is the external capacitor. According to Equations (6) and (7), the design parameters of the first-order stage in Figure 4 are summarized as

$$\omega_{m0} = \frac{K_a g_m}{C} \quad (8)$$

$$\omega_c = \frac{K_b g_m}{C} \quad (9)$$

According to Equations (2)–(4), we could rewrite Equations (8) and (9) as Equations (10) and (11), respectively. They are shown as

$$\omega_{m0} = \sqrt{I_{Ba}} \frac{J_0 \sqrt{I_B}}{C} \quad (10)$$

where $J_0 = \alpha\mu C_{ox}(L/W)_{\text{PolyR1}}\sqrt{(W/L)_{M27}(W/L)_{M13}}$
and

$$\omega_C = \sqrt{I_{Bb}} \frac{J_1 \sqrt{I_B}}{C} \quad (11)$$

where $J_1 = \alpha\mu C_{ox}(L/W)_{\text{PolyR2}}\sqrt{(W/L)_{M41}(W/L)_{M13}}$.
So, both the centre frequency ω_C and the cut-off frequency ω_0 could be electronically adjusted independently by the bias currents I_{Ba} and I_{Bb} .

The IRR, defined as the ratio of the gain of the desired sideband to the suppression of the image sideband, is a key parameter of the polyphase filter [27]. Using Equation (6), the IRR can be derived by

$$\text{IRR}(j\omega) = \left| \frac{H_m(j\omega)}{H_m(-j\omega)} \right| = \frac{\sqrt{\omega_{m0}^2 + (\omega + \omega_C)^2}}{\sqrt{\omega_{m0}^2 + (\omega - \omega_C)^2}} \quad (12)$$

According to Equations (8) and (9), Equation (12) could be rewritten by

$$\text{IRR}(j\omega) = \sqrt{\frac{K_a^2 g_m^2 + (\omega_C + K_b g_m)^2}{K_a^2 g_m^2 + (\omega_C - K_b g_m)^2}} \quad (13)$$

IRR at the centre frequency ω_C could be got as

$$\text{IRR}(\omega_C) = \sqrt{1 + 4 \frac{K_b^2}{K_a^2}} \quad (14)$$

2.3 Non-ideal Characteristics

In actual application, the performance of the proposed circuits may deviate from the ideal by the non-ideal characteristic being used. The following non-ideal characteristics are discussed from the perspectives of parasitics. The simplified equivalent circuit of the non-ideal MOCDTA model is shown in Figure 5.

As Figure 5 depicts, there are parasitic resistances (R_P and R_N) at input terminals P and N , and parasitic resistances and capacitors (R_Z , C_Z , R_{Xa} , C_{Xa} , R_{Xb} , C_{Xb} , and R_X , C_X) from terminal Z , $Xa\pm$, and $Xb\pm$ to ground. $\alpha_P = 1 - \varepsilon_P$, $|\varepsilon_P| \ll 1$ is the current transfer error from P to Z terminals, $\alpha_N = 1 - \varepsilon_N$, $|\varepsilon_N| \ll 1$ is the current transfer error from N to Z terminals, β is the transconductance inaccuracy factor from Z to X terminals, γ_{oa} is the inaccuracy factor of the coefficient K_a from $X\pm$ to $Xa\pm$, and γ_{ob} is the inaccuracy factor of the coefficient K_b from $X\pm$ to $Xb\pm$. In the ideal case, $\alpha_P = \alpha_N = \beta = \gamma_{oa} = \gamma_{ob} = 1$.

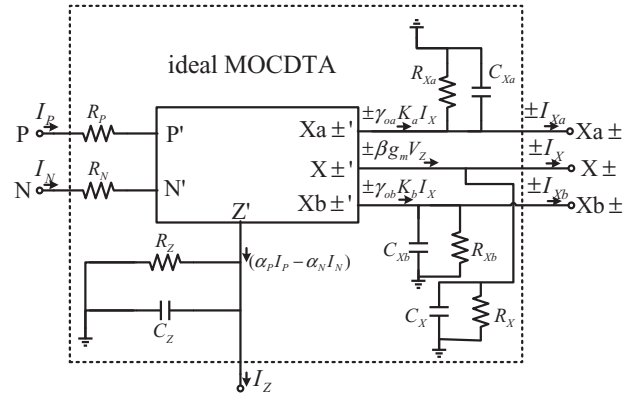


Figure 5: Simplified equivalent circuit of the non-ideal MOCDTA

For simplicity, in the first-order stage which is shown in Figure 4, the parasitic impedances at terminals of MOCDTA1 are taken to be same with the ones at corresponding terminals of MOCDTA2. It is easily observed that the parasitic capacitors C_Z could be absorbed into the external capacitor and the parasitic resistor R_Z at terminal Z would change the type of the impedance which should not be of a purely capacitive character.

In practice, there is $C \gg C_Z$. So, the transfer function of the complex filter which is written by Equation (7) gets modified to

$$H_m(j\omega) \approx \frac{-\alpha_N B \beta g_m}{j\omega C - j\alpha_N B K_b \gamma_{ob} \beta g_m + \alpha_P A K_a \gamma_{oa} \beta g_m + G_Z} \quad (15)$$

where $A = 1/(1 + R_P/R_{Xa} + sC_{Xa}R_P)$ and $B = 1/(1 + R_N/R_{Xb} + sC_{Xb}R_N)$.

According to Equation (15), Equations (8) and (9) could be rewritten by

$$\omega_{m0} = \frac{1/R_Z + \alpha_P \beta \gamma_{oa} A K_a g_m}{C} \quad (16)$$

$$\omega_C = \frac{\alpha_N \beta \gamma_{ob} B K_b g_m}{C} \quad (17)$$

It is clear that both the centre frequency ω_C and cut-off frequency ω_{m0} are affected by the parasitic parameters and hence a good design of MOCDTA should be considered to alleviate the non-ideal effects.

The sensitivities of the cut-off frequency ω_{m0} to the non-idealities and external component are given as

$$S_{\alpha_P, \beta, \gamma_{oa}, g_m, K_a, A}^{\omega_{m0}} < 1, \quad S_{R_Z}^{\omega_{m0}} > -1, \quad S_C^{\omega_{m0}} = -1 \quad (18)$$

$$S_{\alpha_N, \gamma_{ob}, K_b, R_N, R_{Xb}, C_{Xb}}^{\omega_{m0}} = 0 \quad (19)$$

According to the expression of A , we could deduce the formulas as

$$S_{R_p, C_{Xa}}^A < 1, \quad S_{R_{Xa}}^A > -1 \quad (20)$$

so, we could get the equations as

$$S_{R_p, C_{Xa}}^{\omega_{m0}} = S_A^{\omega_{m0}} S_{R_p, C_{Xa}}^A < 1, \quad S_{R_{Xa}}^{\omega_{m0}} = S_A^{\omega_{m0}} S_{R_{Xa}}^A > -1 \quad (21)$$

The sensitivities of the centre frequency ω_C to the non-idealities and external component are also given as

$$S_{\alpha_N, \beta, \gamma_{ob}, g_m, K_b, B}^{\omega_C} = 1, \quad S_C^{\omega_C} = -1, \quad S_{\alpha_p, \gamma_{oa}, K_a, R_p, R_{Xa}, C_{Xa}, R_Z}^{\omega_C} = 0, \\ S_{R_N, C_{Xb}}^{\omega_C} < 1, \quad S_{R_{Xb}}^{\omega_C} > -1 \quad (22)$$

The above equations clearly shown that the sensitivity values are within the range of $|S| \leq 1$, therefore, the sensitivities of first-order stage are low.

2.4 Noise Analysis

Noise performance analysis of the active component MOCDTA is given in this section. The dominant noise sources of CMOS active devices are thermal and flicker noise. In these applications, the flicker noise could be safely neglected due to high work frequencies which are more than 20 MHz. The noise contributed by transistors can be described by a noise current source i_{DS1}^2 , which is between the drain and source of transistors [28]. Considering only thermal noise, we have

$$\overline{i_{DS1}^2} = \frac{8kT}{3} g_{ml} df \quad (23)$$

where g_{ml} is the transconductance of transistor ML , k is the Boltzmann constant, T is the absolute temperature, and df is bandwidth. The output current noise spectral density of the A^2/Hz at Z terminal can be approximated as

$$\overline{i_{Z, \text{out}}^2} \approx \overline{i_{DS10}^2} + \overline{i_{DS8}^2} + \left(g_{m10}^2 + g_{m8}^2 \right) \frac{\overline{i_{DS9}^2} + \overline{i_{DS7}^2}}{g_{m9}^2 + g_{m7}^2} \quad (24)$$

and the output current noise spectral density of the A^2/Hz at X terminal can be approximated as

$$\overline{i_{X, \text{out}}^2} \approx \overline{i_{DS23}^2} + \overline{i_{DS18}^2} + \left(g_{m23}^2 + g_{m18}^2 \right) \left(\frac{\overline{i_{DS22}^2} + \overline{i_{DS19}^2}}{g_{m22}^2 + g_{m19}^2} \right. \\ \left. + \frac{\overline{i_{DS21}^2} + \overline{i_{DS20}^2}}{g_{m21}^2 + g_{m20}^2} \right) + \frac{g_{m23}^2}{g_{m24}^2} \left(\overline{i_{DS13}^2} + \overline{i_{DS24}^2} \right) \\ \left. + \frac{g_{m18}^2}{g_{m17}^2} \left(\overline{i_{DS26}^2} + \overline{i_{DS17}^2} \right) \quad (25)$$

the output current noise spectral density of the A^2/Hz at AX and BX terminal can be approximated as

$$\overline{i_{AX, BX, \text{out}}^2} \approx \overline{i_{DS35}^2} + \overline{i_{DS34}^2} + \frac{g_{m35}^2}{g_{m36}^2} \left(\overline{i_{DS32}^2} + \overline{i_{DS36}^2} \right) \\ + \frac{g_{m34}^2}{g_{m33}^2} \left(\overline{i_{DS33}^2} + \overline{i_{DS40}^2} \right) + \frac{g_{m35}^2}{g_{m37}^2} \left(\overline{i_{DS27}^2} + \overline{i_{DS37}^2} \right) \quad (26)$$

According to Equations (24)–(26), the W/L and bias current which could offer appropriate transconductance to lower output current noise should be considered. From Equation (23), low transconductance could reduce the noise current, which means an increasing overdrive voltage. However, this results in increasing DC supply voltages. Hence, there is a trade-off between noise performance and power consumption. The simulation results of output current noises are given in Section 3.2.

2.5 Current-mode Leapfrog Complex Filter using MOCDTAs

The approach that is utilized to get the leapfrog complex filter is converting the SFD of leapfrog real filter. First, the SFD of the leapfrog structure is shown in Figure 6 [24]. In Figure 6, the leapfrog fourth-order real filter is introduced as example.

Second, we could replace the $g_m Z_k$ ($k = 1, 2, 3$, and 4) with Equation (6). That is to say, the signal flow of $g_m Z_k$ in Figure 6 would be replaced with the signal flow of Figure 3(b). The resultant SFD of the fourth-order leapfrog complex filter is represented in Figure 7. In Figure 7, I_i and Q_i are the quadrature input signals, I_o and Q_o are

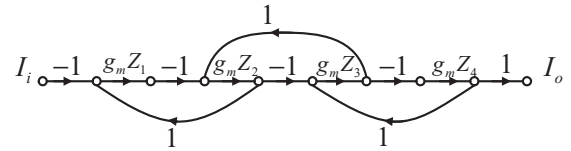


Figure 6: SFD of the leapfrog fourth-order real filter

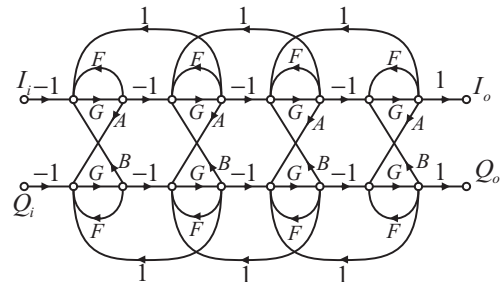


Figure 7: SFD of the leapfrog fourth-order complex filter

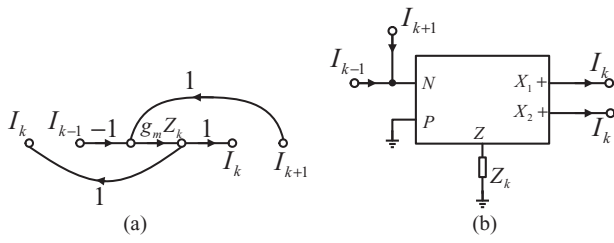


Figure 8: (a) The sub-graph of Figure 6 and (b) their corresponding sub-circuit based on MOCDTA

the quadrature output signals. Q_i could be got through shifting the phase of I_i by 90° .

There are

$$F = -\lambda, \quad G = \frac{\omega_0}{j\omega}, \quad A = -B = \frac{\omega_0}{\omega_C} \quad (27)$$

Through using the symbolic operations with MATLAB, the transfer function of the fourth-order complex filter of Figure 7 could be obtained, which is written by

$$H_{\text{Fourth polyphase}} = \omega_0^4 / [(s - j\omega_C)^4 + 4\lambda\omega_0(s - j\omega_C)^3 + (6\lambda^2\omega_0^2 - 3\omega_0^2)(s - j\omega_C)^2 + (4\lambda^3\omega_0^3 - 6\lambda\omega_0^3)(s - j\omega) + \omega_0^4(1 - 3\lambda^2 + \lambda^4)] \quad (28)$$

where $\omega_0 = \omega_{m0}/\lambda$. From Equation (28), if the $s - j\omega_C$ is recognized as a whole, the fraction would be the transfer function of real low-pass filter. $s - j\omega_C$ denotes the real low-pass filter is transformed to the complex filter. So, the SFD of Figure 7 could be proved to realize the fourth-order complex filter.

Using MOCDTA is suitable for realizing the leapfrog SFD. In Figure 8, the approach to realize the inter-stage circuit is presented. The sub-graph of Figure 6 is shown

in Figure 8(a), and its corresponding MOCDTA-based sub-circuit is shown in Figure 8(b) [24]. Because of current-mode, it is convenient to merge the signal flows. Therefore, using sub-circuits of Figure 8(b) and Figure 4 repeatedly could make up the complete fourth-order leapfrog complex filter which is shown in Figure 9.

3. SIMULATION RESULTS

3.1 Frequency Responses

The characteristics of the proposed circuits have been verified by SPECTRE simulations in CHRT 0.18 μm standard CMOS process. The filter is with $\pm 1.25\text{ V}$ supply. Simulations show that the centre frequency of the filter could be tuned from 20 to 80 MHz. In this process, the impedance of external capacitors is constant which is 4 pF. Two examples are given. The two examples could offer different centre frequencies to satisfy the various situations.

The frequency responses of examples 1 and 2 are shown in Figures 10 and 11, respectively. Example 1 has been designed with $I_{B1} = 40\ \mu\text{A}$, $I_{B2} = 50\ \mu\text{A}$, $I_{B3} = 45\ \mu\text{A}$,

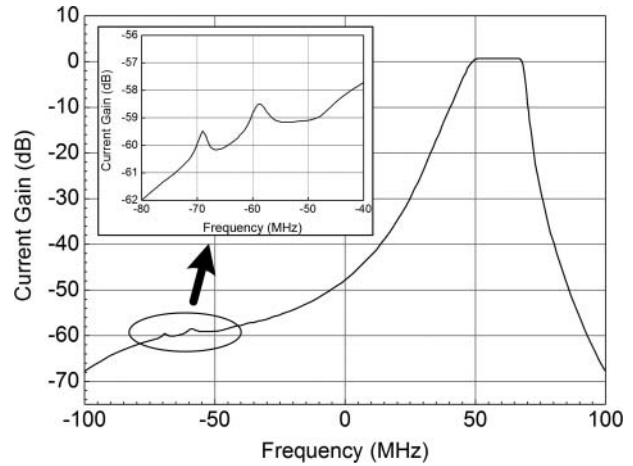


Figure 10: Simulation of frequency response of example 1

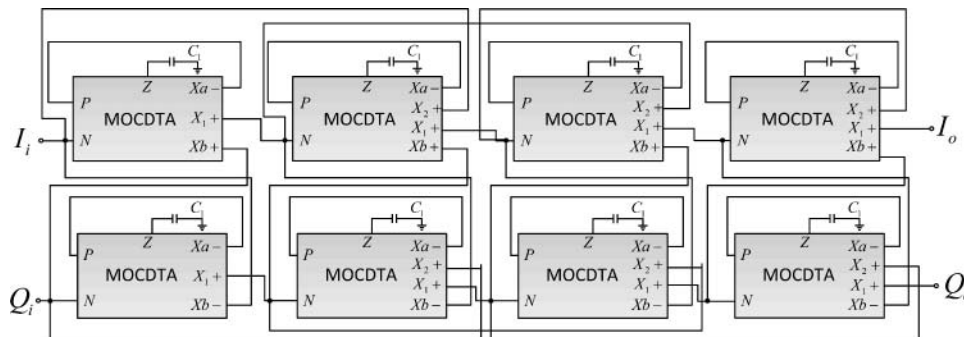


Figure 9: The fourth-order leapfrog complex filter using MOCDTA

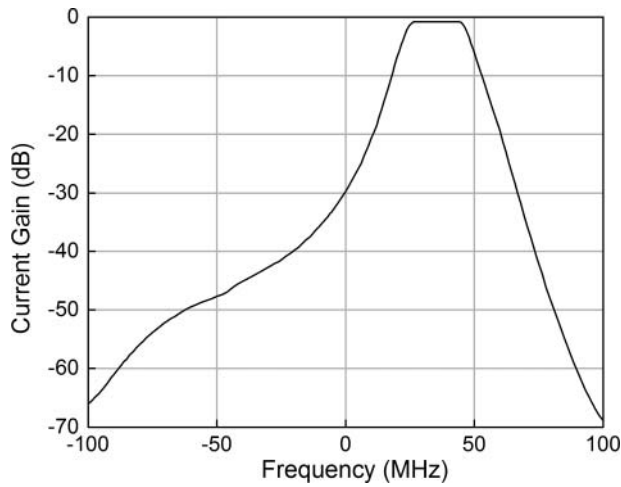


Figure 11: Simulation of frequency response of example 2

$I_{B4} = 60 \mu\text{A}$, $I_{Ba1} = 150 \mu\text{A}$, $I_{Ba2} = 150 \mu\text{A}$, $I_{Ba3} = 155 \mu\text{A}$, $I_{Ba4} = 155 \mu\text{A}$, $I_{Bb1} = 150 \mu\text{A}$, $I_{Bb2} = 150 \mu\text{A}$, $I_{Bb3} = 120 \mu\text{A}$, $I_{Bb4} = 145 \mu\text{A}$, and $C_1 = C_2 = C_3 = C_4 = 4 \text{ pF}$. Its bandwidth is 22.4 MHz which is obtained from 46.1 to 68.5 MHz. The IRR is more than 59 dB. The IIP3 is simulated by applying two-tone signals 58 and 58.5 MHz. The result of the simulation is shown in Figure 12. We can observe that the IIP3 could be 18.58 dBm. Example 2 has been designed with $I_{B1} = 40 \mu\text{A}$, $I_{B2} = 50 \mu\text{A}$, $I_{B3} = 40 \mu\text{A}$, $I_{B4} = 50 \mu\text{A}$, $I_{Ba1} = 80 \mu\text{A}$, $I_{Ba2} = 90 \mu\text{A}$, $I_{Ba3} = 80 \mu\text{A}$, $I_{Ba4} = 90 \mu\text{A}$, $I_{Bb1} = 40 \mu\text{A}$, $I_{Bb2} = 100 \mu\text{A}$, $I_{Bb3} = 40 \mu\text{A}$, $I_{Bb4} = 95 \mu\text{A}$, and $C_1 = C_2 = C_3 = C_4 = 4 \text{ pF}$. Its bandwidth is 26.1 MHz which is obtained from 22.3 to 48.4 MHz. The IRR is more than 39 dB. The IIP3 is simulated by applying two-tone signals 34 and 33.5 MHz. The result of the simulation is shown in Figure 13. We can observe that the IIP3 is 19.02 dBm.

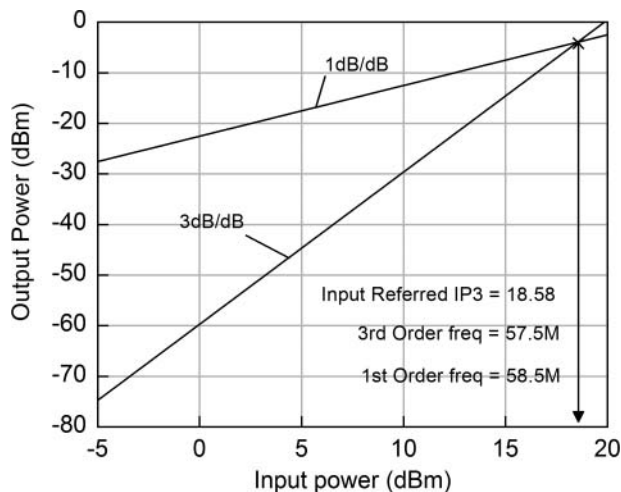


Figure 12: Simulation of in-band IIP3 of example 1

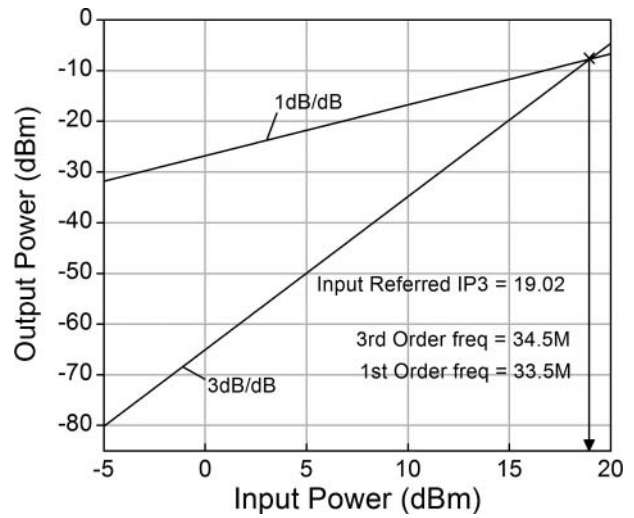


Figure 13: Simulation of in-band IIP3 of example 2

The detailed parameters of the two examples are listed in Table 2. The proposed examples offer high centre frequency and high bandwidth. To highlight the advantages, the proposed filter would be compared with other complex filters which shown in Table 3. In Table 3, we can observe that the proposed filter has significant advantages in the tunability among high centre frequencies and wide bandwidth, which is suitable for the gradual higher IF in the RF receivers. Meanwhile, the filters could possess good linearity.

3.2 Output Noise

The output noise is concerned, and the simulation results are shown in Figure 14. The results show that the output noise presents a low value over the entire passband. The output noises of ports AX and BX are both 22.8 pA/sqrt (Hz) at 10 MHz, the output noises of ports X and Z are

Table 2: The detailed parameters of the examples

Spec.	Order	Passband (MHz)	Bandwidth (MHz)	IRR (dB)	IIP3 (dBm)	Power supply (V)
Example 1	4	46.1–68.5	22.4	>59 dB	18.58	2.5
Example 2	4	22.3–48.4	26.1	>39 dB	19.02	2.5

Table 3: The comparison between the proposed filter and previous works

Spec.	Order	Centre Frequency (MHz)	Bandwidth (MHz)	IRR (dB)	IIP3 (dBm)	Power supply (V)
Example 1	4	57.3	22.4	>59	18.58	2.5
Example 2	4	35.4	26.1	>39	19.02	2.5
[1]	6	2	2.5	28.2	15.11	1.5
[11]	6	3	1	>54	29.2	2.7
[14]	7	3	1	>53	15.6	2.3
[21]	3	1	1	>28	9	3.3
[23]	4	0.5	0.9	28	22.6	1.8

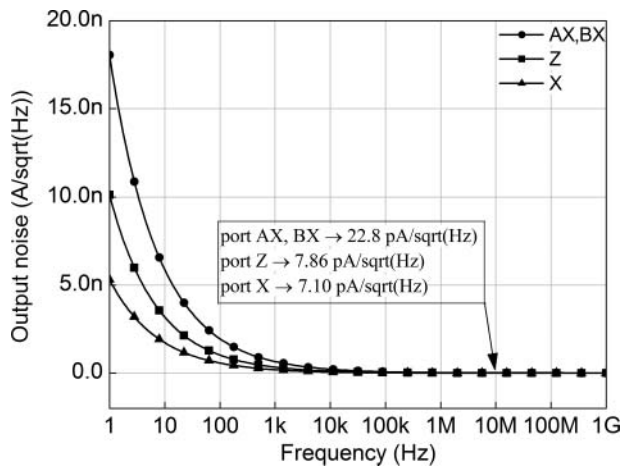


Figure 14: Output noise of ports of MOCDTA

7.10 and 7.86 pA/sqrt(Hz), respectively. So, the output noise is even lower over the work frequencies from 20 to 70 MHz in these examples.

3.3 Temperature Effects

Temperature effects on the filter are included, and the simulated results are given in Figure 15. In Figure 15, we try to analyse temperature fluctuation of example 2 from -4 to 72 °C, and the changes of responses are provided. We could find that they are shifted to high frequency with decreasing temperatures. During this process, the shape of the responses would change. Near the right cut-off frequencies, a peak would exist in the response as the temperature is too low, and a fall would turn up in the response as the temperature is too high. Near -40 MHz, the responses have small change. To achieve detailed changes near the nominal temperature which is 27 °C, we analysed some parameters under the temperature fluctuation about 30% from 27 °C. It means the temperatures are approximately from 20 to 35 °C. The

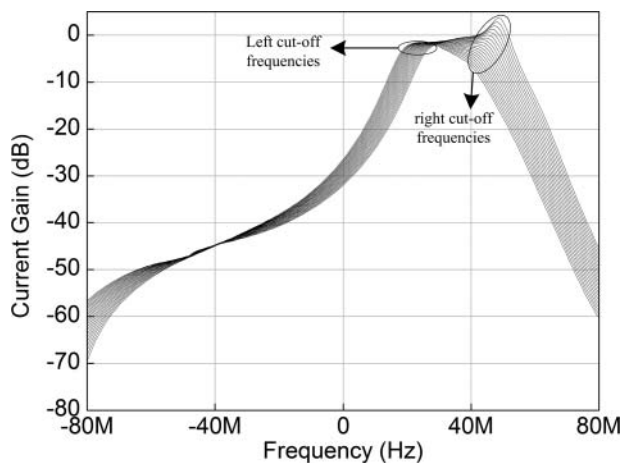


Figure 15: The amplitude-frequency responses from -4 to 72 °C

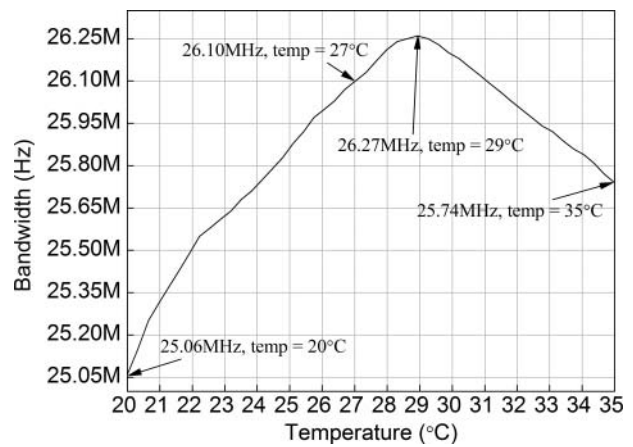


Figure 16: Temperature effect on bandwidth

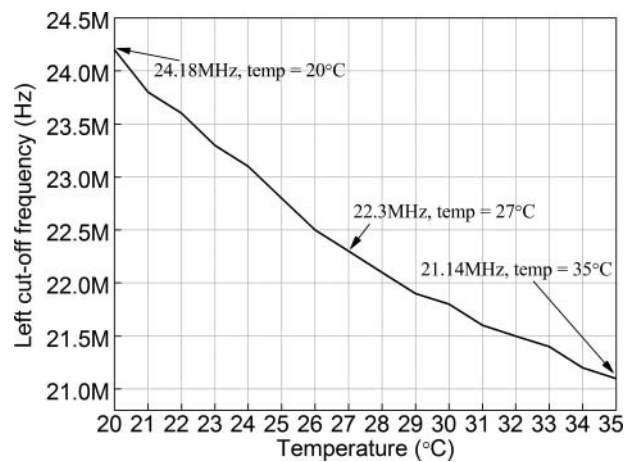


Figure 17: Temperature effect on left cut-off frequencies

bandwidth, left cut-off frequencies, and IRR change slightly, which are shown in Figures 16–18. We could find that the fluctuations of bandwidth, left cut-off frequency, and IRR are 3.98%, 8.43%, and 1.79%, respectively.

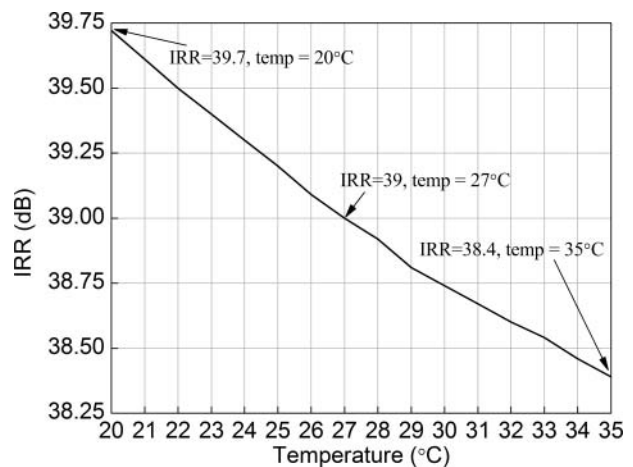


Figure 18: Temperature effect on IRR

4. CONCLUSION

In this paper, a new fourth-order complex filter based on MOCDTA is presented, which utilizes the leapfrog structure. The proposed work has some advantages. First, the proposed fourth-order filter requires eight MOCDTAs and eight passive components for current-mode realizations. This is to say, that use the method in this work could make the n th-order complex filter in this work just need $2n$ MOCDTAs and $2n$ passive components. Second, the current-mode leapfrog structure in this work has high output impedance and low input impedance. Third, the proposed filter is realized without resistors, and all the external capacitors are grounded, which is suitable for integrated circuit (IC) technology. Fourth, because of the characteristic of the MOCDTA, the centre frequency of the proposed filter could be dozens megahertz. Fifth, the wide bandwidth could be obtained, which could be more than 20 MHz. Sixth, the centre frequency and the bandwidth could be electrically adjustable with external bias currents.

ACKNOWLEDGMENTS

This work was supported in part by the National Natural Science Foundation of China (No. 61274020). We would like to thank the authors whose works we have cited throughout our paper and also thank the individuals who reviewed this article and gave valuable comments.

DISCLOSURE STATEMENT

No potential conflict of interest by reported by the authors.

FUNDING

National Natural Science Foundation of China [grant number 61274020].

REFERENCES

1. C. Laoudias and C. Psychalinos, "1.5-V complex filters using current mirrors," *IEEE Trans. Circuits Syst II, Exp. Briefs*, vol. 58(9), pp. 575–579, **Sept. 2011**.
2. Z. Xiaoxing, N. Xiayu, I. Masahiro, and K. Noriyoshi, "Realization of universal active complex filters using CCII and CFCCII," *Analog Integrated Circuits and Signal Processing*, vol. 81(2), pp. 129–137, **Aug. 1999**.
3. H. Alzahrer and M. Alghamdi, "A CMOS bandpass filter for low-IF Bluetooth receivers," *IEEE Trans. Circuits Syst. I*, vol. 53(8), pp. 1636–1647, **Aug. 2006**.
4. H. Alzahrer, M. Alghamdi, and M. Ismail, "CMOS low-power bandpass IF filter for Bluetooth," *IET Circuits Devices Syst.*, vol. 1(1), pp. 7–12, **Feb. 2007**.
5. X. Zhang, N. Kambayashi, and Y. Shinada, "A realization of active current-mode resonator with complex coefficients using CCII," *IEICE Trans. Fundam.*, vol. 80(2), pp. 413–415, **Feb. 1997**.
6. A. M. Abuelma'atti and M. T. Abuelma'atti, "A current-conveyor-based polyphase filter," *WSEAS Trans. Electron.*, vol. 4, pp. 656–663, **2005**.
7. S. Shahrani and M. Gahtani, "A new polyphase current-mode filter using digitally-programmable CCCII," in *Proceedings Of the 18th International Conference Microelectronics*, Dhahran, **Dec. 2006**, pp. 142–145.
8. M. T. Abuelma'atti and S. M. Al-Shahrani, "A new poly-phase currentmode filter using programmable-gain current-controlled current-conveyor," *WSEAS Trans. Electron.*, vol. 2, pp. 138–141, **2005**.
9. M. Un, "Implementation of polyphase filter section with CFAs," *Frequenz*, vol. 58, pp. 221–224, **Sept. 2004**.
10. M. T. Abuelma'atti and S. M. Al-Shahrani, "A new poly-phase mixed mode bandpass filter section using current feedback operational amplifier," *WSEAS Trans. Electron.*, vol. 2, pp. 128–131, **2005**.
11. H. Alzahrer and N. Tasadduq, "A CMOS low power current-mode polyphase filter," in *Proceedings of the IEEE International Symposium Low Power Electronics Design*, San Francisco, **Aug. 2009**, pp. 75–79.
12. P. Andreani and S. Mattisson, "On the use of Nauta's transconductor in low-frequency CMOS-C bandpass filters," *IEEE J. Solid-State Circuits*, vol. 37(2), pp. 114–124, **Feb. 2002**.
13. P. Andreani, S. Mattisson, and B. Essink, "A CMOS gm-C polyphase filter with high image band rejection," in *Proceedings of the ESSCIR*, Stockholm, **Sept. 2000**, pp. 244–247.
14. B. Shi, W. Shan, and P. Andreani, "A 57-dB image band rejection CMOS-C polyphase filter with automatic frequency tuning for Bluetooth," in *Proceedings of the ISCAS*, May 2002, pp. V-169–II-172.
15. B. Guthrie, J. Hughes, T. Sayers, and A. Spencer, "A CMOS gyrator low-IF filter for a dual-mode Bluetooth/ZigBee transceiver," *IEEE J. Solid-State Circuits*, vol. 40(9), pp. 1872–1878, **Sept. 2005**.
16. C. Psychalinos, "Low-voltage log-domain complex filters," *IEEE Trans. Circuits Syst. II, Exp. Briefs*, vol. 55(11), pp. 3404–3412, **Dec. 2008**.
17. J. Hughes, A. Spencer, A. Worapishet, and R. Sitdhikorn, "1 mW CMOS polyphase channel filter for Bluetooth," *Proc. IEE Circuits Devices Syst.*, vol. 149, pp. 348–354, **Oct. 2002**.
18. J. Mahattanakul and P. Kumsat, "Structure of complex elliptic Gm–C filters suitable for fully differential implementation," *IET Circuits Devices Syst.*, vol. 1(4), pp. 275–282, **Aug. 2007**.
19. M. Tedeschi, A. Liscidini, and R. Castello, "Low-power quadrature receivers for ZigBee (IEEE 802.15.4) applications," *IEEE J. Solid-State Circuits*, vol. 45(9), pp. 1710–1719, **Sept. 2010**.
20. W. Chuanchuan, L. Zhiqun, and H. Ningbing, "A CMOS Gm–C complex filter with on-chip automatic tuning for wireless sensor network application," *J. Semicond.*, vol. 32(5), pp. 05002-1–05002-6, **May 2011**.
21. C. Xin, Z. Lungui, Y. Haigang, L. Fei, and G. Tongqiang, "A pseudo differential Gm–C complex filter with frequency tuning for IEEE802.15.4 applications," *J. Semicond.*, vol. 32(7), pp. 075005-1–075005-8, **July 2011**.
22. C. Laoudias and C. Psychalinos, "Low-voltage Bluetooth/ZigBee complex filter using current mirrors," in *Proceedings of the ISCAS*, Paris, **May 2010**, pp. 1268–1271.

23. M. Zhou, J. Wu, C. Chen, and Z. Cai, "A tunable Gm-C polyphase filter with high linearity and automatic frequency calibration," *IEICE Electron. Express*, vol. 11(18), pp. 1–6, **Sept. 2014**.
24. U. E. Ayten, M. Sagbas, and H. Sedef, "Current mode leapfrog ladder filters using a new active block," *AEU-Int. J. Electron. Commun.*, vol. 64(6), pp. 503–511, **June 2010**.
25. D. Biolek, "CDTA—building block for current-mode analog signal processing," in *Proceedings of the ECCTD03*, vol. III, Krakow, **2003**, pp. 397–400.
26. D. Biolek, A. U. Keskin, and V. Biolkova, "Quadrature oscillator using CDTA-based integrators," *WSEAS Trans. Electron.*, vol. 153(3), pp. 463–469, **2006**.
27. J. Kaukavuori and K. Stadius, "Analysis and design of passive polyphase filters," *IEEE Trans. Circuits Syst. I, Reg. Papers*, vol. 55(10), pp. 3023–3037, **May 2008**.
28. E. Bruun, "Noise properties of CMOS current conveyors," in *Proceedings of the IEEE International Symposium on ISCAS, Atlanta*, **May 1996**, vol. 1, pp. 144–147.

Authors



Hao Peng received the BS degree in 2013. Now he is studying towards the MS degree at the Hunan University. His research includes design and simulation of current-mode integrated circuits.

E-mail: devin7960@hnu.edu.cn



Chunhua Wang was born in Yongzhou, China, in 1963. He received the PhD degree from Beijing University of Technology, Beijing, China. He is currently a professor of Hunan University, Changsha, China. His research includes current-mode circuit design and RFIC design. He is the corresponding author.

E-mail: wch1227164@hnu.edu.cn



Xiaotong Tian is studying towards the BS degree at the Hunan University.

E-mail: 912758847@qq.com



Jun Liu is a professor of engineering. He is an engineer at the STATE GRID HUNAN electric power company. His main research interests include optical communications' wireless communications' next-generation networking, and internet.

E-mail: 82706@qq.com
